Effect of strain and electric field on the electronic soft matter in manganite thin films

Tara Dhakal, Jacob Tosado, and Amlan Biswas
Department of Physics, University of Florida, Gainesville, FL 32611
(Dated: February 6, 2008)

We have studied the effect of substrate-induced strain on the properties of the hole-doped manganite $(La_{1-y}Pr_y)_{0.67}Ca_{0.33}MnO_3$ (y = 0.4, 0.5 and 0.6) in order to distinguish between the roles played by long-range strain interactions and quenched atomic disorder in forming the micrometer-scale phase separated state. We show that a fluid phase separated (FPS) state is formed at intermediate temperatures similar to the strain-liquid state in bulk compounds, which can be converted to a metallic state by applying an external electric field. In contrast to bulk compounds, at low temperatures a strain stabilized ferromagnetic metallic (FMM) state is formed in the $y = 0.4$ and 0.5 samples. However, in the $y = 0.6$ sample a static phase separated (SPS) state is formed similar to the strain-glass phase in bulk compounds. Hence, we show that long-range strain interaction plays a dominant role in forming the micrometer-scale phase separated state in manganite thin films.

PACS numbers: 75.47.Lx, 73.50.Fq, 75.47.Gk, 75.70.-i

Multiphase coexistence in hole-doped manganites is a result of the competition between phases of different electronic, magnetic and structural orders [1, 2]. This competition leads to large changes in the physical properties of manganites due to small perturbations e.g. colossal negative magnetoresistance (CMR). At low temperatures the two competing phases are the ferromagnetic metallic (FMM) and charge-ordered insulating (COI) phases. In manganites with greater average A-site cation radii ($\langle r_A \rangle$) and consequently a larger effective one-electron bandwidth (W) (e.g. $La_{1-x}Ca_xMnO_3$, $0.2 < x < 0.5$), the pseudocubic FMM phase is favored at low temperatures [3]. When smaller ions such as Pr are substituted at the A-site, $\langle r_A \rangle$ and W are reduced. In these compounds the double-exchange mechanism is suppressed and hence the pseudotetragonal (distorted) COI phase has a comparable free energy to the FMM phase, resulting in micrometer scale phase separation [4]. It was shown that in the presence of quenched disorder introduced by the ions of different radii, the similarity of the free energies leads to coexistence of the two competing phases [2]. However, the observation of martensitic strain accommodation in manganites [5] and fluid-like growth of the FMM phase observed in magnetic force microscopy (MFM) images of phase separated manganites [6], suggests that the phases are not pinned. In fact, due to this behavior the phase separated state in manganites has been described as an "electronic soft matter" state [2, 7]. These observations can be explained by an alternative model which shows that the different crystal structures of the FMM and COI phases generate long range strain interactions leading to an intrinsic elastic energy landscape, which leads to micrometer scale phase separation even without quenched disorder [1]. To understand the underlying mechanism for micrometer scale phase separation in manganites, it is essential to distinguish between the roles played by quenched disorder and long range strain interactions. We can then devise protocols to manipulate this phase separated state with external parameters such as strain, electric field, light etc., and propose possible technical applications.

If long range strain interactions are the principal cause of phase coexistence then it should be possible to control the elastic energy landscape with substrate induced strain, which is known to dramatically affect the nature of structural transitions in materials such as shape memory alloys and ferroelectrics [8]. On the other hand, the effect of quenched disorder can be estimated from the effect of isovalent substitution of La-ions by Pr-ions. In this paper we report our results on the effect of substrate induced strain and isovalent substitution in thin films of the manganite $(La_{1-y}Pr_y)_{0.67}Ca_{0.33}MnO_3$ (LPCMO), and compare our results to bulk LPCMO. The $T - H$ phase diagram of bulk LPCMO clearly shows two distinct types of phase separation (PS), a strain-liquid (dynamic PS) and a strain-glass (frozen PS) regions [9]. The strain-liquid phase shows large fluctuations in resistivity and a slow relaxation of the magnetization [9]. We show that in thin films of LPCMO, a fluid phase separated (FPS) state is formed at intermediate temperatures similar to the strain-liquid state in bulk materials. However, a strain stabilized FMM phase is formed at low temperatures leading to a sharper and larger drop in resistivity compared to bulk samples. This strain stabilized FMM phase transforms to a static phase separated (SPS) state when the Pr content is increased. The SPS state is analogous to the strain-glass state in bulk LPCMO. An external electric field transforms the FPS state to a metallic state. However, there is negligible electric field effect once the sample reaches the SPS state.

We have grown thin films of $(La_{1-y}Pr_y)_{0.67}Ca_{0.33}MnO_3$ (LPCMO) (y=0.4, 0.5 and 0.6) using pulsed laser deposition (PLD). The films were grown in an oxygen atmosphere of 420 mTorr on $NdGaO_3$ (NGO) (110) substrate kept at 820°C. All the films described in this letter are 30 nm thick and were

grown at a rate of about 0.05 nm/s. These growth conditions were optimized to obtain an insulator-to-metal transition temperature while cooling, T_{IM} (cooling), close to that observed in bulk compounds of similar composition and the minimum transition width at T_{IM} (cooling). Such an optimization is crucial for mapping the phase diagram of LPCMO, since the properties of thin films of this compound vary markedly depending on the growth conditions. Standard $\theta - 2\theta$ x-ray diffraction data show that the films are epitaxial and of a single chemical phase. Since the resistance of the films can be as high as 1 GΩ, the resistivity ρ, of the films was measured with a two-probe method using a constant voltage source, as shown in the lower inset of Fig. 1(a), with V_0 set at 5 V [10]. For the ρ vs. T curves, the temperature was varied at a rate of 2 K/min.

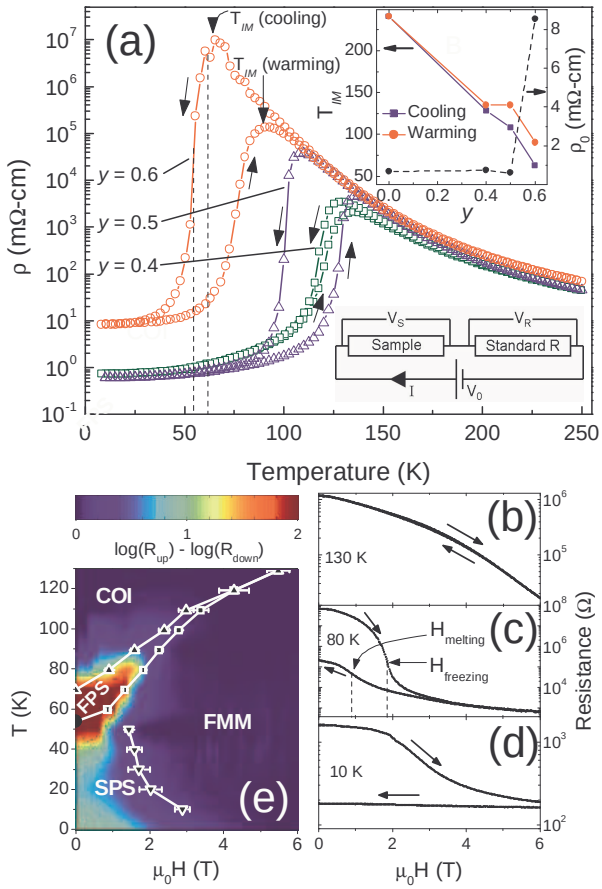

FIG. 1: (color online) (a) Resistivity vs. temperature curves for thin films of $(La_{1-y}Pr_y)_{0.67}Ca_{0.33}MnO_3$ (y = 0.4, 05, and 0.6). Cooling and warming directions are indicated by arrows. The dotted lines mark the range of temperatures for the $I-V$ curves shown in fig. 2. The upper inset shows the variation of the transition temperatures and low temperature resistivity (ρ_0) with y. The lower inset shows the setup for measuring the two probe resistance using a constant voltage source. (b), (c), and (d) R vs H curves for the y = 0.6 sample in the cooling cycle. (e) The $T - H$ phase diagram for the y = 0.6 thin film in the cooling cycle.

The ρ vs. T data for three LPCMO films (y = 0.4, 0.5, and 0.6) are shown in Fig. 1(a). An expected reduction of T_{IM} (cooling) is observed with increasing Pr concentration due to the reduction of $\langle r_A \rangle$. The width of the hysteresis between warming and cooling cycles of temperature drops sharply when y is reduced from 0.5 to 0.4 (Fig. 1(a), top inset). A remarkable feature of the resistivity is that, unlike in bulk LPCMO [4], the residual resistivity ρ_0, (measured at 10 K) does not change from $y = 0$ ($La_{0.67}Ca_{0.33}MnO_3$, LCMO) to $y = 0.5$ and then rises sharply for $y = 0.6$ (Fig. 1(a), top inset). Resistivity measurements have been used to construct temperature-magnetic field ($T - H$) phase diagrams, which elucidate the stability of phases in manganites [9]. To illustrate the effect of substrate induced strain on the properties of LPCMO, we mapped the $T - H$ phase diagram of the $y = 0.6$ sample by measuring resistance R vs. H curves at different temperatures for the cooling cycle (Fig. 1(b) to 1(d)). Since the effect of H is irreversible, the sample was reset after every field sweep by heating it to 150 K and then cooling it to the set temperature. The data points were obtained by locating the magnetic field corresponding to the steepest change in R at a given temperature i.e. where dR/dH is maximum (Fig. 1(c)). The squares and triangles represent the melting and freezing fields respectively (Fig. 1(e)). The melting field line is extended to zero field by including the T_{IM} (cooling) at zero field from Fig. 1(a). The inverted triangles represent the melting field at low temperature ($T \leq 50$ K). Since the transitions widths can be large in thin films (Fig. 1(d)), as shown by the error bars in Fig. 1(e), we have used a more direct method of constructing the $T - H$ phase diagram. We plotted the difference in $\log(R)$ between up sweep and down sweep of H $\log(R_{up})$-$\log(R_{down})$, in the $T - H$ plane as a 2D color plot (Fig. 1(e)). The two methods of plotting the phase diagram give similar results except for the SPS region due to the broad transition with magnetic field at low temperatures. Four distinct regions can be clearly identified in this phase diagram. Two pure phases namely the COI state and the FMM state and two mixed phase states namely, the fluid phase separated (FPS) state and the static phase separated (SPS). The nomenclature of the mixed phase states is based on the electric field effect, which will be explained in detail in the following sections.

To elucidate the nature of phase coexistence in our thin films of LPCMO we have to understand the combined effect of substrate induced strain and Pr-substitution. Our LPCMO samples were grown on NGO (110) substrates which are known to stabilize the pseudocubic FMM phase in LCMO [6]. Conversely, Pr has a smaller cation radius than La and hence, substitution of La-ions by Pr-ions favors a distorted crystal structure [11]. The distortion produced by Pr-substitution reduces the T_{IM} (cooling) in our LPCMO thin films similar to bulk LPCMO [4]. On

the other hand, strain induced by the NGO substrate removes the resistivity anomaly at the charge-ordering temperature (T_{CO}) seen in bulk LPCMO [4], which is an effect of the suppression of the bulk structural transition near T_{CO} [12]. It has been shown for ferroelectric thin films that when the structural transition is suppressed due to substrate strain, there is a strain build-up in the film, which is released by the formation of domains with different structures [13]. A similar structural separation in manganites would lead to phase separation into FMM and COI regions and the observed reduction of T_{IM} (cooling). Furthermore, the thermal contraction of the substrate modifies the strain landscape leading to the fluid nature of the phases as has been observed in MFM images of LPCMO thin films [14]. A detailed temperature dependent structural study of the thin films is required to verify the above hypothesis. However, it is clear from Fig. 1(a) and 1(e) that in spite of substrate induced strain, the phase diagram of the LPCMO ($y = 0.6$) sample is similar to that of bulk LPCMO [9].

In contrast to the $y = 0.6$ sample, ρ_0 for the $y = 0.4$ and 0.5 samples drops to a value consistent with the pure FMM phase of the $y = 0$ sample (Fig. 1(a), upper inset). Magnetization measurements also show that the $y = 0.5$ sample has a saturation magnetization (M_{sat}) consistent with a pure FMM phase [15]. Hence, these two samples have a pure FMM phase at low temperatures in contrast to the strain-glass phase observed in bulk LPCMO [9], because the NGO substrate favors the pseudocubic FMM phase at low temperatures. When the Pr-concentration is increased to $y = 0.6$, ρ_0 increases by about an order of magnitude to 8.7 mΩ-cm. The value of M_{sat} for this sample is consistent with 50% of the material being in the FMM phase at low temperatures. As shown in Fig. 1(e), a phase similar to the strain glass phase in bulk LPCMO (the SPS state) appears in the phase diagram of thin film LPCMO only when the Pr-concentration is increased to $y = 0.6$. It was suggested in ref. [9] that the strain-liquid to strain-glass transition is due to the interaction of the long-range strain with the quenched atomic disorder. The observation of the FPS state and the absence of the SPS state in the $y = 0.5$ sample show that under substrate induced strain, long-range strain is the driving force behind micrometer scale phase separation in manganites.

To realize potential applications, an accessible handle is needed to manipulate the phase separation in these thin films and one candidate is an external electric field. Previous measurements of the electric field effect showed a large drop in the resistivity of charge-ordered manganites on the application of an electric field [16]. Electric field effects have also been observed in thin films of LPCMO [17]. Large electric current effects have been observed in LPCMO crystals due to Joule heating of the metallic regions [18].

The voltage was applied to the LPCMO thin films using two indium contacts 0.75 mm apart. The circuit for measuring the $I - V$ curves is the same as the one used for measuring resistivity [10]. Figure 2(a) shows the $I - V$ curves for the $y = 0.6$ sample for the cooling run. At a threshold voltage V_{th}, the current across the film rises abruptly. This electric field effect is irreversible as shown for the 59 K curve in figure 2a. The sample stays in the low resistance state even when the electric field is removed. To recover the high resistance state we heat the film to a temperature above the resistivity hysteresis region and then cool it down to the next desired temperature. We have plotted the quantity $\log(\mathrm{d}I/\mathrm{d}V)$ calculated from these $I - V$ curves as a function of temperature and voltage to construct a $T - V$ phase diagram as shown in Fig. 2(b). The observed electric field effect is not a heating effect as reported by Tokunaga *et al.* [18] since heating should increase the resistance in the temperature range shown in Fig. 2(a). We also observed a similar electric field effect while cooling the $y = 0.5$ sample.

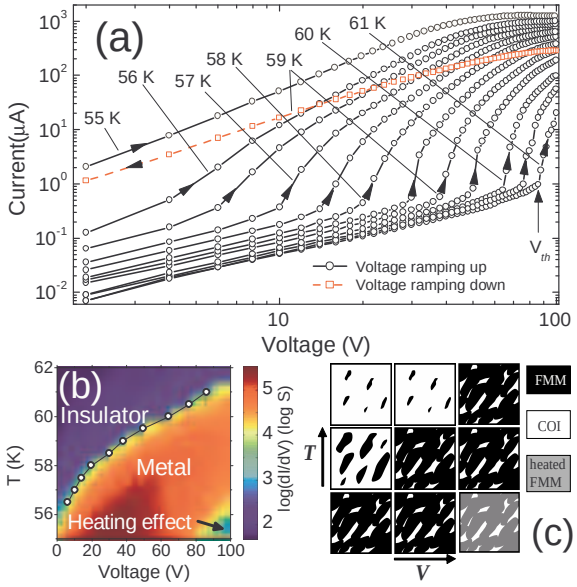

FIG. 2: (color online) (a) $I - V$ curves of the $(La_{1-y}Pr_y)_{0.67}Ca_{0.33}MnO_3$ ($y = 0.6$) thin film in the cooling cycle with the voltage being ramped up. The dashed curve is the $I - V$ curve at 59 K with the voltage being ramped down. (b) The $T - V$ phase diagram for the $y = 0.6$ thin film, showing the variation of V_{th} with temperature and the heating effect at high voltages and low temperatures, in the cooling cycle. (c) Schematic representation of the phase coexistence in the $T - V$ plane.

A recent theoretical study using an extended double exchange Hamiltonian showed that the application of an electric field favors the FMM phase over the COI phase [19]. The authors also performed a numerical calculation using a random resistor network to model a two-phase manganite sample, with low resistances representing the metallic regions and high resistances for the insulating

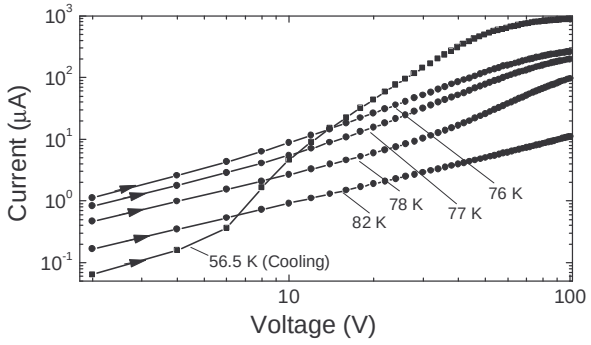

FIG. 3: $I-V$ curves of the $(La_{1-y}Pr_y)_{0.67}Ca_{0.33}MnO_3$ (y = 0.6) thin film in the warming cycle with the voltage being ramped up. The $I-V$ curve at 56.5 K for the cooling cycle is shown for comparison.

regions. The electric field converts the high resistances to low resistances and a percolation of the metallic regions leads to the insulator to metal transition at V_{th}. V_{th} decreases as the number of high resistance elements is decreased from a 100% to 50% of the sample, which qualitatively agrees with the observed variation of V_{th} as a function of temperature shown in Fig. 2(b) (decreasing temperature is analogous to decreasing number of high resistances). A schematic picture of the phase coexistence in LPCMO for the cooling cycle in the $T-V$ plane is shown in Fig. 2(c). As the size of the metallic regions (shown in black) increases, the electric field across the smaller insulating regions (shown in white) is enhanced, enhancing the local electric field across the insulating regions. This enhancement of the local electric field leads to the predicted and observed decrease in V_{th} with decreasing temperature. Above V_{th}, percolation of the metallic regions in the film results in the sharp rise in the conductivity of the film. Further rise in the voltage across the film increases the current flowing through the metallic regions resulting in local heating and a consequent decrease in conductivity similar to the results of ref. [18]. This heating effect is clearly seen in the bottom right corner of the $T-V$ phase diagram in Fig. 2(b) (gray regions in Fig. 2(c)). When the sample is cooled down to the SPS state, the metallic regions form a percolating path. Hence, in the SPS state increasing the voltage across the sample results in a larger current and Joule heating.

No sharp increase in current was observed during the warming run as shown in Fig. 3. The $I-V$ behavior during cooling for a similar resistance value is shown for comparison. In the warming run, the absence of a V_{th} suggests that there is no enhancement of the local electric field. An explanation for this effect can be found in MFM measurements, which have shown that the FMM regions are static in the warming run [14]. Therefore, once the sample is cooled to the SPS region, the FMM and COI phases are locked in space. Since the FMM regions percolate through the sample, application of a voltage leads to Joule heating of the FMM regions. On further warming the FMM regions homogeneously transform to a high temperature insulating phase and hence there is no local enhancement of the electric field.

In conclusion, substrate induced strain modifies the mechanism of micrometer-scale phase separation in manganites. At intermediate temperatures ($T \sim T_{IM}$ (cooling)), long-range strain interactions lead to a fluid phase separated state analogous to the strain-liquid phase in bulk LPCMO [9]. However, below a critical Pr concentration ($y \leq 0.5$) the FPS state transforms to a strain stabilized FMM phase at low temperatures, unlike the strain-liquid to strain-glass transition in bulk LPCMO [9]. A static phase separated state analogous to the strain-glass phase in bulk LPCMO is observed at low temperatures only when the Pr concentration (and hence the quenched atomic disorder) is increased above a critical value ($y \geq 0.6$). An external electric field provides an effective means to modify the phase separation in manganites since it lowers the resistance of the FPS state by two orders of magnitude due to a local electric field enhancement. However, an electric field has negligible effect on the SPS state. Further experiments using low temperature MFM are needed to find the microscopic mechanism of the electric field effect.

[1] K. H. Ahn *et al.*, Nature **428**, 401 (2004).
[2] E.Dagotto, Science **309**, 257 (2005).
[3] H. Y. Hwang *et al.*, Phys. Rev. Lett. **75**, 914 (1995).
[4] M. Uehara *et al.*, Nature **399**, 560 (1999).
[5] V. Podzorov *et al.*, Phys. Rev. B **64**, 140406 (2001).
[6] Amlan Biswas *et al.*, Phys. Rev. B **61**, 9665 (2000); Amlan Biswas *et al.*, *ibid.* **63**, 184424 (2001).
[7] G.C. Milward *et al.*, Nature **433**, 607 (2005).
[8] Y. L. Li *et al.*, Acta Materialia **50**, 395 (2002).
[9] P. A. Sharma *et al.*, Phys. Rev. B **71**, 224416 (2005); L. Ghivelder *et al.*, *ibid.* **71**, 184425 (2005).
[10] We measured the voltage V_R across the standard resistor R. The current in the circuit then was V_R/R and the voltage across the sample $V_S = V_0 - V_R$. Hence, the sample resistance $R_S = (V_0 - V_R) \times R/V_R$. As a check, the low temperature resistivity was also measured using a standard four-probe method. The $I-V$ curves were measured by varying V_0.
[11] D. E. Cox *et al.*, Phys. Rev. B **57**, 3305 (1998).
[12] Prellier *et al.*, Appl. Phys. Lett. **75**, 397 (1999).
[13] W. Pompe *et al.*, J. Appl. Phys. **74**, 6012 (1993).
[14] Liuwan Zhang *et al.*, Science **298**, 805 (2002).
[15] M_{sat} is estimated by measuring the $M-H$ loops for the thin films and then subtracting the paramagnetic background due to the NGO substrate.
[16] A. Asamitsu *et al.*, Nature **388**, 50 (1997).
[17] N. Pandey *et al.*, Phys. Rev. B **67**, 054413 (2003).
[18] M. Tokunaga *et al.*, Phys. Rev. Lett. **93**, 037203 (2004); M. Tokunaga *et al.*, *ibid.* **94**, 157203 (2005).
[19] R. Gu *et al.*, Phys. Rev. B **67**, 153101 (2003).